Research Article | Vol. 28, No. 8 / 13 April 2020 / Optics Express 11742

Optics EXPRESS

Atmospheric correction for satellite-derived bathymetry in the Caribbean waters: from a single image to multi-temporal approaches using Sentinel-2A/B

ISABEL CABALLERO[1,*] AND RICHARD P. STUMPF[2]

[1]Instituto de Ciencias Marinas de Andalucía (ICMAN), Consejo Superior de Investigaciones Científicas (CSIC), Avenida República Saharaui, Cadiz, 11510, Spain
[2]National Centers for Coastal Ocean Science, NOAA National Ocean Service, East West Highway, 1305, Silver Spring, MD 20910, USA
[*]isabel.caballero@icman.csic.es

Abstract: Different atmospheric correction (AC) procedures for Sentinel-2 satellites are evaluated for their effectiveness in retrieving consistent satellite-derived bathymetry (SDB) over two islands in the Caribbean (Buck and Culebra). The log-ratio method for SDB, which allows use of minimal calibration information from lidar surveys (25 points in this study), is applied to several Sentinel-2A/B scenes at 10 m spatial resolution. The overall performance during a one-year study period depends on the image quality and AC. Three AC processors were evaluated: ACOLITE Exponential model (EXP), ACOLITE Dark Spectrum Fitting model (DSF), and C2RCC model. ACOLITE EXP and ACOLITE DSF produce greater consistency and repeatability with accurate results in a scene-by-scene analysis (mean errors ~1.1 m) for depths up to 23 m (limit of lidar surveys). In contrast, C2RCC produces lower accuracy and noisier results with generally higher (>50%) errors (mean errors ~2.2 m), but it is able to retrieve depth for scenes in Buck Island that have moderately severe sunglint. Furthermore, we demonstrate that a multi-temporal compositing model for SDB mapping, using ACOLITE for the input scenes, could achieve overall median errors <1 m for depths ranging 0-23 m. The simple and effective compositing model can considerably enhance coastal SDB estimates with high reliability and no missing data, outperforming the traditional single image approaches and thus eliminating the need to evaluate individual scenes. The consistency in the output from the AC correction indicates the potential for automated application of the multi-scene compositing technique, which can apply the open and free Sentinel-2 data set for the benefit of operational and scientific investigations.

1. Introduction

The global seascape, with more than 1.5 million kilometers of coastline, is key in supporting Earth's interconnected land and marine ecosystems [1]. The coastal zones are densely populated, accounting for about 39% of the total population residing within 100 km from the coast, and provide significant environmental, economic and societal services [2]. The dynamic seacoast environments can see substantial morphological modifications due to short-term (extreme meteo-oceanographic events) and long-term (seasonal changes in the wave climate, erosion/accretion, and currents) [3]. In addition, coastal ecosystems are considered amongst the most threatened environments due to climate change, sea level rise, and anthropogenic phenomena [4]. Bathymetry, the depth of the sea bottom, is a critical parameter in maritime spatial planning, used for effective coastal resource management, industry, navigation, defense, aquaculture, tourism, and other purposes. However, the depth of the ocean has been determined over less than 18% of the seafloor using echo-sounders at a resolution of about 1 km [5]. There remains a global lack of nearshore bathymetry information called the "white gaps" [6]. Continuous monitoring of

#390316 https://doi.org/10.1364/OE.390316
Journal © 2020 Received 11 Feb 2020; revised 25 Mar 2020; accepted 26 Mar 2020; published 6 Apr 2020

Optics EXPRESS

the seabed morphology and its alterations has become a critical need of scientists, coastal planners, and resource managers. The recognition of the importance of seafloor mapping has been highlighted during last few years, leading to many national and international initiatives to better understand our shallow regions [7]. Increasing demand exists for updated and detailed bathymetric information of shallow areas with higher spatio-temporal coverage and adequate vertical and horizontal accuracies [8]. This objective requires efficient and cost-effective new strategies compared to the conventional costly and logistically complex ship-borne (multibeam) or airborne-based (lidar) surveys [9,10].

During the last four decades, multispectral satellite technologies have been examined as an alternative to traditional depth measurements [10]. Mapping bathymetry from optical satellite imagery, satellite-derived bathymetry (SDB), is mainly conducted in optically shallow water, typically at depth lower than 30 m, where light reflected off the bottom returns to the satellite. Several SDB approaches have been developed for depth estimation in shallow waters [11–14]. Novel methodological strategies have been implemented as a result of the new constellations of higher spatial, temporal, and radiometric resolution satellite sensors [15–19]. These satellite observations have emerged as a cost-effective strategy for rapid and efficient high-resolution mapping. However, SDB is subject to the challenging tradeoff between spectral, spatial and temporal resolution, the last one limiting the availability of cloud-free images, particularly in tropical coastal regions with frequent cloud cover.

The Sentinel-2A/B twin-satellite mission from the Copernicus programme has established a new era in coastal mapping due to its routine acquisition frequency of 5 days at the equator, high spatial resolution of 10 m, and its free and open data access policy [20,21]. The Sentinel-2 mission is based on a constellation of two identical satellites in the same orbit, phased at 180° to each other. Both satellites, -2A and -2B provide an optimal coverage of Earth's land surfaces, large islands as well as inland and coastal waters. While the mission was engineered mainly for terrestrial applications, their imaging sensor features match the ones proposed by the coastal and inland remote sensing community for accurate and effective coastal seabed monitoring. Owing to the technical capabilities offered by the Sentinel-2 fleet, scientists have begun to take into consideration this mission as a suitable solution to map bathymetry [16,22–25].

The availability of 5-day temporal resolution allows the selection of the most qualitatively suitable images within the desired timeframe. Individual scenes are inevitably affected by external features such as clouds and their shadows, sunglint, waves, boats and their wakes, and particularly, the local water quality, and these problems have not yet been adequately addressed for routine mapping. The standard solution to this problem is manual inspection of imagery to find an optimal scene, a cumbersome and not necessarily effective approach. Selecting a scene with potentially high reliability and no missing data is challenging, especially for large or optically or physically complex areas. Multiple sources of uncertainty need to be examined in order to select a scene suitable for SDB. This critical analysis of many images must consider sun-satellite geometry, anticipated wave height and direction, as well as clouds, glint, and water turbidity variations [17]. As example, Botha et al. [26] demonstrated that higher total environmental noise due to increased surface glint and higher atmospheric path-scattering yield lower performance with underestimation of depths. A shift from single-image to multi-temporal methods is a potential solution to these sources of error. Few works have already indicated the potential of multi-scene approaches in order to select either a superior scene, or to combine images to eliminate noise [16,18,19,27,28] as well compositing to reduce turbidity impacts on SDB [29]. Recent studies suggested the potential of multi-temporal approaches over clear waters: Chu et al. proposed a time-domain noise removal method to create an optimal image from the time series of Sentinel-2 [27] whereas Sagawa et al. used random forest machine learning and multi-temporal satellite images to create a generalized depth estimation model with Landsat-8 [19].

Optics EXPRESS

Atmospheric Correction (AC) is a critical step in the use of multi-scene SDB approaches; they may improve retrieval of bathymetric information, however, they require consistent retrievals of water reflectance. Noise introduced by atmospheric and air-water interface effects may reduce multi-scene performance if not fully corrected [30,31]. An error in the AC associated with the estimation of the Remote Sensing Reflectance (Rrs) generates uncertainties through the atmospheric path scattering and water surface reflectance (i.e., sunglint) [26,32]. AC error becomes especially important in multi-temporal studies, because the images must be directly comparable to avoid compromising the results [25]. In this context, testing AC algorithms to define the best performance is an essential piece of SDB monitoring. Several open source AC solutions have been developed for Sentinel-2, such as the ACOLITE processor developed by the Royal Belgian Institute of Natural Sciences [33–37] and the Case 2 Regional CoastColour processor (C2RCC) originally developed by Doerffer and Schiller [38,39].

The aim of this study was to explore the suitability and consistency of these two AC processors, ACOLITE and C2RCC, for coastal SDB applications using Sentinel-2A/B data, in conjunction with one of the most widely adopted models for bathymetry extraction [13]. These strategies were evaluated in two tropical study areas around Buck and Culebra Islands, in the northeast Caribbean waters (Fig. 1), for several single scenes during one year. The potential of the AC processors for SDB has been reported individually in other studies [24,25,29,40]. In this investigation, we focused on the comparison of the different AC methods to derive consistently accurate bathymetry. As AC consistency will be a key source of error in any multi-scene method (in order to address clouds, glint, turbidity, etc.), we also examined the use of the AC solutions in a multi-temporal SDB compositing approach [29] to define its performance compared to individual scenes. Error distribution after validation with lidar surveys was calculated to describe the quality of the retrieved SDB for both single and multi-temporal approaches.

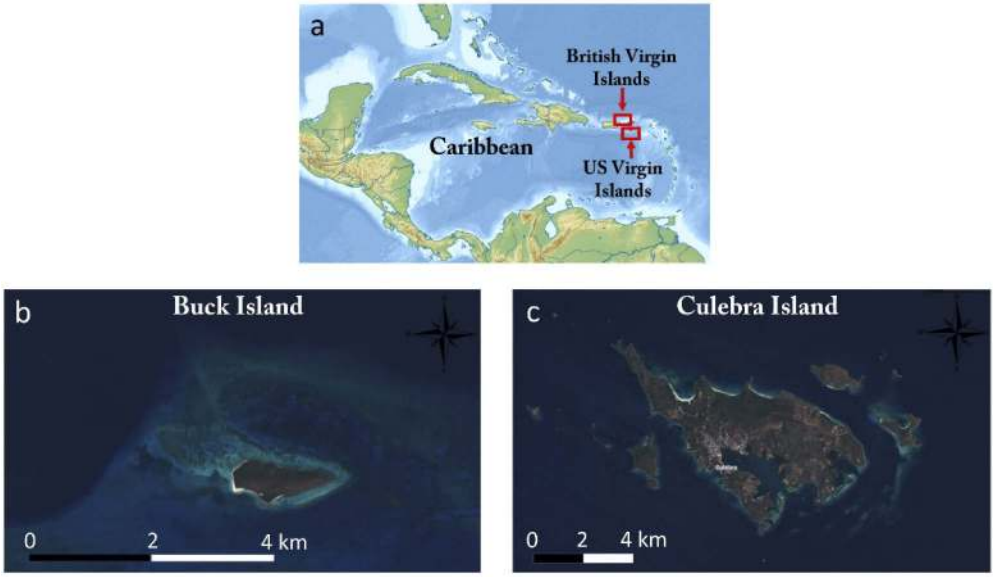

Fig. 1. a) Location of the study regions in the Caribbean waters and Sentinel-2 images at 10 m spatial resolution b) over Buck Island in the US Virgin Islands, and c) over Culebra Island in the British Virgin Islands.

Optics EXPRESS

2. Materials and methods

2.1. Lidar data

The National Geodetic Survey (NGS) obtained topographic and bathymetric (topobathy) airborne lidar bathymetry (ALB) in July-August 2018 over two tropical islands located in the northeast Caribbean waters: Buck Island and Culebra Island (Fig. 1) after Hurricane Maria (September 2017). These data were collected by the Joint Airborne Lidar Bathymetry Technical Center of Expertise (JALBTCX) using the Coastal Zone Mapping and Imaging Lidar (CZMIL) system, owned and operated by the U.S. Army Corps of Engineers (USACE). The system collects topobathy lidar data at 10 kHz and RGB imagery at 2 Hz. A CASI-1500 hyperspectral line scanner is integrated with the system as well. Anomalous high and/or low elevation values have been flagged and removed, and point cloud classification algorithms have been validated via manual review and QA/QC. Horizontal positions were provided in geographic coordinates, referenced to the North American Datum of 1983 National Adjustment of 2011 (NAD83 NA11). Vertical positions were provided in ellipsoid elevations and in meters. The vertical and horizontal accuracy of these datasets are 10 cm and 100 cm, respectively at 95% confidence level. Bathymetric lidar coverage extends from the shoreline offshore 250 meters or to laser extinction, whichever occurs first. Gaps may exist in the data coverage, arising due to a number of operational and environmental conditions, including but not limited to, airspace restrictions, high terrain, active surf, low-reflectivity bottom substrate materials and turbidity in the water column.

Culebra Island is located 27 km off northeastern Puerto Rico in the British Virgin Islands [Fig. 1(c)]. ALB data in Culebra corresponded to optically shallow waters ranging from 0 up to 23 m, with seagrass beds as the most abundant community type, followed by coral reefs, sandy bottoms and hard bottom (pavement) [41]. In the US Virgin Islands [Fig. 1(b)] depths surveyed in Buck Island ranged from 0 up to 23 m, and habitat type includes coral reef, hard bottom, seagrasses, and unconsolidated sediment [42]. These regions are characterized by clear waters and contain several bottom irregularities that were detectable with ALB, allowing the examination of the MSI capacity to map these bottom types. The high-resolution ALB observations (1 m spatial resolution) were selected as the reference in the well-controlled study sites and compared to SDB products. ALB data sets were referenced to the mean lower low water (MLLW) and gridded at the MSI's image resolution (10 m).

2.2. Sentinel-2A/B images and atmospheric correction

This study used the Sentinel-2A and 2B twin polar-orbiting satellites (launched, respectively, in June 2015, and March 2017) that were developed by the European Space Agency (ESA) and the European Commission to meet the operational needs of the Copernicus programme. The multispectral instruments (MSI) on-board both satellites are now operational. The radiometric, spectral and spatial characteristics of the bands used in this study are specified in the User Handbook [20]. Sentinel-2 Level-1C products were downloaded from the Sentinel's Scientific Data Hub and images of zone 20 in Buck (sub-tile QLE) and in Culebra (sub-tile QKF) regions were used. Level-1C Sentinel-2 images are geo-located within two pixels (20 m) which is within the stated quality requirements for absolute geo-location [21]. The study period of one year was selected based on lidar collection, with a total number of 18 and 11 Sentinel-2A/B scenes available in Buck and Culebra Islands, respectively (see Appendix for detailed information on the Sentinel-2 images used). The manual intervention for this step was only associated with the selection of the scenes with low cloud coverage (<20%). During late spring and summer, there was a severe sunglint contamination over the study regions, in particular for tiles located in the eastern side of the swath.

Before the application of the bathymetric model, all the images were atmospherically corrected. Currently, several open source atmospheric correction algorithms are available for Sentinel-2. In

Optics EXPRESS

this study, images were processed to Level-2A (L2A) with two of the most common software, which officially support Sentinel-2 data: 1) ACOLITE processor, and 2) the Case 2 Regional CoastColour processor (C2RCC). Both algorithms used an image-based approach, without the requirement of in-situ atmospheric information. The Sen2Cor and iCOR software were also initially tested but due to their low performance (especially computation efficiency, but also low accuracy), results were not further included in this study. Recent SDB studies also indicated poorer consistency of both processors in comparing between in-situ depth and log-transformed reflectance band ratios [25]. In addition, since the current status of SeaDAS does not officially support Sentinel-2 processing, and the SeaDAS l2gen AC only outputs 20 m resolution data from MSI, we excluded this processor for our comparison exercise.

ACOLITE was specifically developed for marine, coastal, and inland waters in the Royal Belgian Institute of Natural Sciences (RBINS), which supports free processing, specifically for aquatic applications, of both Landsat-8 and Sentinel-2 [35]. We selected two different algorithms within the ACOLITE toolbox. The first, Exponential model (EXP) corresponded to a combination of the Near-Infrared (NIR) and Short Wave Infrared (SWIR) channels (865/1600 nm) for the aerosol correction with a user defined epsilon value, typically a maritime aerosol=1 [33,34]. This strategy has been shown to significantly improve the quality of the products by minimizing the influence of NIR/SWIR instrument noise [43], but did not include glint correction. Recent studies demonstrated the accuracy and consistency of this method for SDB in several areas of USA [24,29]. Recently, a novel AC algorithm within ACOLITE, the Dark Spectrum Fitting (DSF) atmospheric correction has been implemented [36]. This approach addresses some of the common problems of the Exponential model with a robust automated band selection process, and an aerosol correction, which allows for spatial variability of aerosols (both type and concentration) without affecting the noise level in the output product. The DSF was originally developed for water applications of "very high resolution" metre-scale optical satellites but showed potential for the application to MSI [37], due to their better spectral coverage (notably including bands in the SWIR region). In this study, we also selected the DSF AC using the optional image based sunglint correction and masking of the total surface reflectance with the following parameters: (dsf_path_reflectance = tiled, l2w_mask_threshold=0.05, l2w_mask_negative_rhow = False). ACOLITE products corresponded to Remote Sensing Reflectance (Rrs, sr^{-1}) in all visible and NIR bands resampled to 10 m pixel size.

The Case 2 Regional CoastColour (C2RCC) processor, originally developed by Doerffer and Schiller [38], uses a large database of radiative transfer simulations inverted by neural networks as basic technology. Through the ESA Data User Element (DUE) CoastColour Project, major improvements focused on a five component bio-optical model and a coastal aerosol model were introduced [39]. Neural networks are trained in order to perform the inversion of spectrum for the atmospheric correction, i.e. the determination of the water leaving radiance from the top of atmosphere (TOA), as well as the retrieval of inherent optical properties of the waterbody [39]. It is applicable to all past and current ocean colour sensors as well as Sentinel-2. It has been validated in various studies and is available through the European Space Agency (ESA)'s Sentinel toolbox in the Sentinel Application Platform (SNAP). It is also used in the Sentinel-3 ground segment processor of ESA for the generation of the Case 2 water products, as well as in the processor for the upcoming MERIS 4th reprocessing. Previous resampling to 10 m for all bands was accomplished in SNAP. Output option as Rrs was selected in our case.

A further spatial filter (median filter 3×3) was conducted on the corrected bands in order to remove some noise and inter-pixel variability. Recent experience with Sentinel-2 imagery indicated spatial filtering reduces noise in the bathymetric products with minimal smoothing (unlike averaging filters) [23,24], as well as with other satellites [44]. The performance and consistency of each algorithms was evaluated specifically for application to bathymetry, rather than for total spectral radiometric accuracy, due to the absence of in-situ radiometric measurements.

Optics EXPRESS

2.3. Satellite-derived bathymetry

The log-transformed band ratio model, widely used algorithm for the estimation of SDB, was tested using the "SDBgreen" approach [13,24], the ratio of blue (490 nm) to green (560 nm) bands, as this combination has been most used in the recent literature [25,27,28,45–52]. The pseudo (relative) SDB (pSDB) retrieved from the satellite were tuned to actual depth using a linear transform and few calibration points (25) from the ALB. The offset coefficient provided an adjustment to the reference bathymetric datum (MLLW) of the reference ALB, implicitly correcting for tide (micro-tidal system). Each scene was tuned separately, with correlation (coefficient of determination, r^2) calculated as a quality indicator.

In addition, a multi-temporal evaluation was accomplished with an automated approach selecting the best pixel along the time series [29]. As turbidity and other noising effects (cloud shadows, glint, bubbles, waves) produce a false shoaling [17,26], the pseudoSDB or pSDB maps (prior to the vertical calibration) were determined for all available scenes. All scenes were compared to identify the maximum pseudoSDB or pSDB at each pixel (after the noise filter was applied), and a resultant composite image was created with the maximum pSDBgreen per pixel. We can presume that the terrain did not change during the one-year study period as there were no major storms impacting the islands after Hurricane Maria (September 2017).

The study regions in the Caribbean needed to have minimal variability in water quality during the study period to conduct the AC comparisons over multiple scenes. These islands are a good choice for having relatively small variations in water clarity. These areas of the islands do not have local sources of material or fresh water inputs, so local sources of nutrients and associated algal blooms or turbidity vary little. Without storms, turbidity from resuspension remains small. Every few years, colored dissolved organic matter from the Orinoco River in South America crosses the Caribbean to these islands. Inspection of ocean color imagery from the NASA ocean biology page (https://oceancolor.gsfc.nasa.gov/) confirmed that this was not occurring during the study period.

The AC performance was assessed through a validation of SDB against lidar. This assessment was conducted by comparing metrics between scenes, by evaluating a single vertical (depth) calibration across scenes, and by evaluating the multi-temporal composite product. The calibrations were compared with slope and r^2. SDB accuracy was determined by validation against in-situ lidar data with the calculation of the bias, mean absolute error (MAE), and median absolute error (MedAE) for each image or product, as well as computing the variation in these metrics across all the scenes.

3. Results

3.1. Buck Island

The different AC processors showed similar results among the images in Buck Island. The distribution of slopes for the vertical calibration of each image suggested analogous values were found for ACOLITE EXP and DSF with mean slopes ~36 whereas lower slopes were found for C2RCC ~30 (Table 1). This difference suggests that ACOLITE and C2RCC have a relative bias against each other in one of the two bands (blue or green); a question that could be best investigated in a study of spectral characteristics of the ACs. The coefficient of variation (CV) shows similar values for EXP and C2RCC (~15%) whereas DSF had more variation in slopes (CV ~35%). The Appendix provides detailed information on the Sentinel-2A/B images selected for Buck Island, the calibration coefficient for the vertical referencing and the coefficient of determination (r^2) as a measure of quality assurance. The r^2 values ranged from 0.92-0.98 and 0.9-0.98 for EXP and DSF, whereas lower values 0.52-0.96 were associated to C2RCC. Some scenes in Buck Island using ACOLITE EXP or DSF were masked out due to intense sunglint

Optics EXPRESS

(scenes 7-10 for both models, scene 13 also for EXP). Tide range is microtidal in this region, so that was not a factor in intercept variation.

Table 1. Descriptive statistics parameters of the slopes from the vertical calibration in the SDB model for each atmospheric correction method in Buck and Culebra Island (see Appendix for a list of Sentinel-2A/B scenes used in this study). The scene number 4 on 2 October 2018 was eliminated for ACOLITE EXP and DSF in Culebra Island. Whereas ACOLITE DSF and C2RCC included a sunglint correction, ACOLITE EXP does not have this option.

Buck	ACOLITE EXP	ACOLITE DSF (sunglint correction)	C2RCC (sunglint correction)	Culebra	ACOLITE EXP	ACOLITE DSF (sunglint correction)	C2RCC (sunglint correction)
Mean	35.75	36.5	29.55	Mean	31	26.7	21.5
Median	35.27	34.5	30.2	Median	31.2	27.2	20.5
Max	50.1	71.8	36.7	Max	35.5	32.4	33.2
Min	27.9	25.1	19.6	Min	24.2	15.8	1.1
SD	5.89	12.9	4.49	SD	3.2	4.5	6.8
CV (%)	16.5	35	15	CV (%)	10.3	16.8	31
Range	22.1	46	17.1	Range	11.3	16.6	23.1

For the retrieved depths at Buck Island, ACOLITE EXP and DSF had comparable performances, with respective ranges of mean bias of 0.12 m and 0.4 m, and MedAE of 0.91 m and 0.86 m (Table 2), generating consistent results for all depth ranges up to 23 m (the Appendix presents accuracy assessment results for each of the individual scenes). Higher errors (>45%) were found for C2RCC with mean MedAE of 1.42 m and bias of 0.26 m (Table 2). This issue with C2RCC was also visible in the scatterplots of lidar against SDB; a clear example of an optimal scene acquired on 9 February 2018 shows higher dispersion for C2RCC compared to both ACOLITE models (Fig. 2). The majority of the points follow the 1:1 line, indicating a general pattern of high accuracy. Histograms also indicated normal distribution of errors for both ACOLITE models while C2RCC presented a skewed and long-tailed error distribution. ACOLITE EXP was more consistent in the whole dataset whereas C2RCC provided lower consistency.

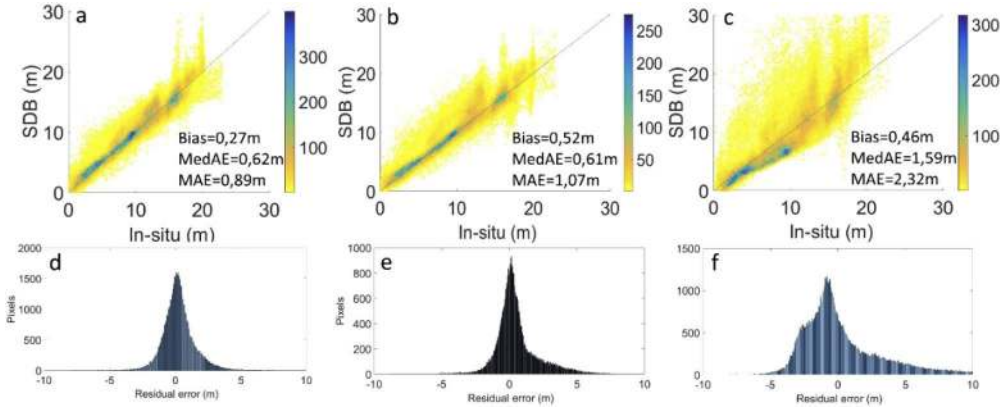

Fig. 2. Examples of scatters for the validation of individual SDB images in Buck Island using a Sentinel-2A image acquired on 9 February 2018 after the Atmospheric Correction a) ACOLITE EXP, b) ACOLITE DSF, and c) C2RCC; and histogram of residuals for d) ACOLITE EXP, e) ACOLITE DSF, and f) C2RCC.

We also applied a single vertical calibration to all scenes. Assuming uniform clear water in this area, ACs should produce consistent results across scenes with a common calibration.

Optics EXPRESS

Table 2. Summary table with mean and standard deviation (SD) statistics of biases and MedAE for all the scenes and the three AC methods using a scene-by-scene calibration or a unique single calibration in Buck Island.

	ACOLITE	EXP	ACOLITE	DSF	C2RCC	
Buck Island	Scene-by-scene calibration	Single calibration	Scene-by-scene calibration	Single calibration	Scene-by-scene calibration	Single calibration
Mean of scene biases (m)	0.12	-0.79	0.4	-1.2	0.26	0.72
SD of scene biases (m)	0.63	1.05	0.35	1.26	0.85	1.18
Mean of scene MedAE (m)	0.91	1.37	0.86	1.74	1.42	1.53
SD of scene MedAE (m)	0.25	0.57	0.41	1.12	0.27	0.28

The vertical calibration from a high quality image acquired on 6 March 2018 was used as the reference. This single calibration produced mean MedAE of 1.37 m, 1.74 m, 1.53 m and MAE of 1.55 m, 1.96 m, 2.1 m using EXP, DSF, and C2RCC models, respectively (Table 2 and Appendix). The single calibration errors were only about 30-40% greater than those obtained from individual scene calibration for depths up to 23 m, indicating good performance by the ACs given the simple assessment approach. Another main finding is that C2RCC retrieved depths during intense sunglint as can be observed in scenes number 7-10 (10-25 May, 14 June, and 13 August) while neither EXP nor DSF retrieved data. The C2RCC results for those glinted scenes are shown in the scatterplots of SDB against lidar data (Fig. 3). With MAE varying from 1.69 m to 2.32 m, the results look similar to the C2RCC performance for non-glinted scenes [Fig. 2(c)].

The multi-temporal compositing approach improved the performance for the ACOLITE models relative to the C2RCC as can be seen in the smaller data scatter [Figs. 4(a), 4(c)], and metrics with bias of 0.37 m and 0.19 m, and MedAE of 0.6 m and 0.74 m for EXP and DSF, respectively (using 13 scenes), whereas much higher errors [Fig. 4(e)] were found for C2RCC with bias of -0.92 m and MedAE of 1.97 m (using the 13 scenes corresponding to ACOLITE, see Appendix for a detailed information on images). The composite using C2RCC and the 5 scenes with severe sun glint performed similarly to C2RCC without sunglint [Fig. 4(g)]. The results show that C2RCC is inferior to ACOLITE for SDB retrieval and is noticeably noisier with the same scenes (13 images) and with the glinted scenes (5 images). However, if other limitations (like clouds) necessitate using scenes that have severe sunglint, C2RCC may be the necessary option, as it produces equivalent error (noise) with or without glint. The vertical calibration also indicated better performance for EXP (30.7x-28, r^2=0.98) and DSF (26.7x-24, r^2=0.96) than for C2RCC (16.7x-13, r^2=0.52), mainly due to the noisy results. The quality of the models is shown in the histogram of the residual errors, with a symmetric distribution for ACOLITE [Figs. 4(b), 4(d)]. However, for C2RCC there are bias problems in its distribution, with a bimodal error distribution, a combination of negative bias for the bulk at greater depths, but a strongly positively skewed error [Figs. 4(f), 4(h)]. This information is significant for selecting the AC algorithm used in SDB mapping, suggesting both ACOLITE models retrieved higher consistency compared to C2RCC.

These results demonstrate that, by using the multi-temporal approach after ACOLITE, inspection and selection of the best scenes are not necessary. ACOLITE produced consistent results across scenes. Although the 9 February 2018 image had good accuracy [Figs. 2(a), 2(b)], and might be selected as one of the optimal scenes for analysis, the composite solution scheme efficiently described the nearshore depth with good precision [Figs. 4(a), 4(c)]. This area has low turbidity, so compositing may produce only modest localized improvements in quality, as

Optics EXPRESS

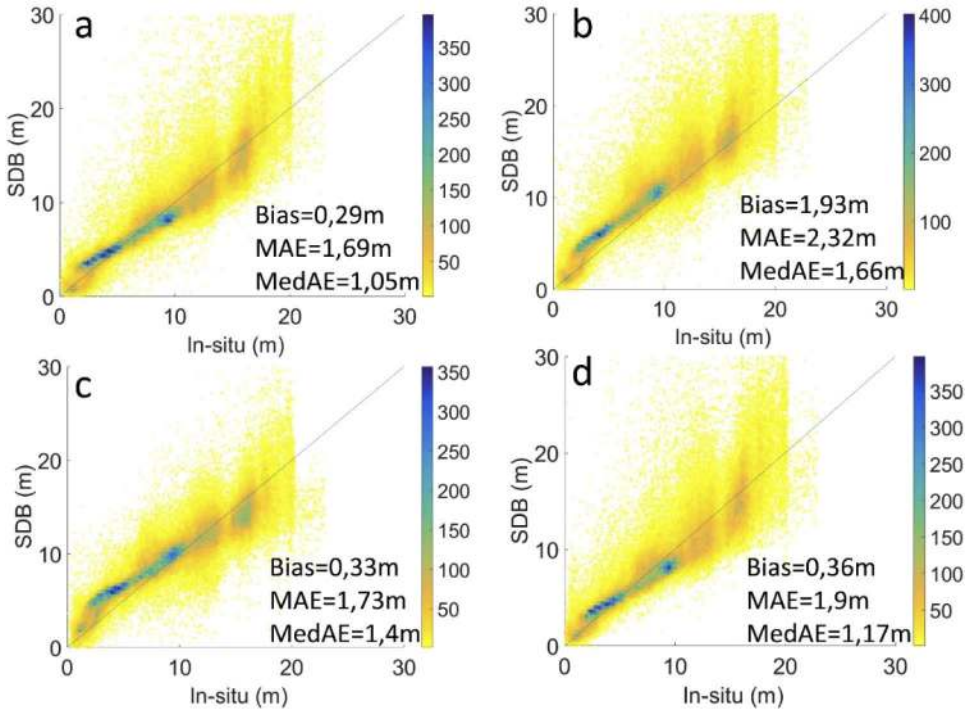

Fig. 3. Validation of individual SDB images in Buck Island for severe sunglint scenes during 2018 after the C2RCC processor on a) 10 May, b) 25 May, c) 14 June, and d) 13 August.

compared to many areas with spatially transient turbidity. Using only a single scene for SDB would produce a more limited or poorer quality data set owing to the various factors that limit data availability and quality: clouds, clouds shadows, sunglint, bubbles, waves, or other artifacts and noise, whereas the multi-temporal strategy addresses these issues.

The compositing method also exhibited some advantages over the in-situ data. The lidar survey was limited, and some water areas nearshore were not retrieved [Fig. 5(a)]. In contrast, by using multiple dates of imagery, features could be identified by the composited SDB maps data along the entire coastal fringe around the island [Figs. 5(b)–5(d)]. The visual analysis of the resulting maps showed qualitatively good agreement with those identifiable in the lidar survey, although much more spatial information is available in the SDB product. SDB can also be used to distinctly recognize shallow coastal geomorphology features located in the northern part of the island. Moreover, the SDB data can identify the position of the shelf boundary, where the coastal shelf drops abruptly or gradually to the optically deep open ocean. In offshore areas, the bottom was not visible and the attributed cut-off depth was ~23 m with saturated depths higher than this (indicated with dark blue in Fig. 5).

3.2. Culebra Island

The results were similar at Culebra as at Buck Island (Table 3). The Appendix provides a list of Sentinel-2A/B images selected for Culebra Island, the calibration coefficient for the vertical referencing and the Coefficient of Determination (r^2) as a measure of quality assurance (Table 4). The distribution of slopes for the vertical calibration shows higher mean slopes of 31 and 26.7 for EXP and DSF, respectively, and lower for C2RCC with 21.5, equivalent to Buck Island outcomes (Table 1). The r^2 of the vertical calibration ranged from 0.88-0.99 and 0.84-0.98 for

Optics EXPRESS

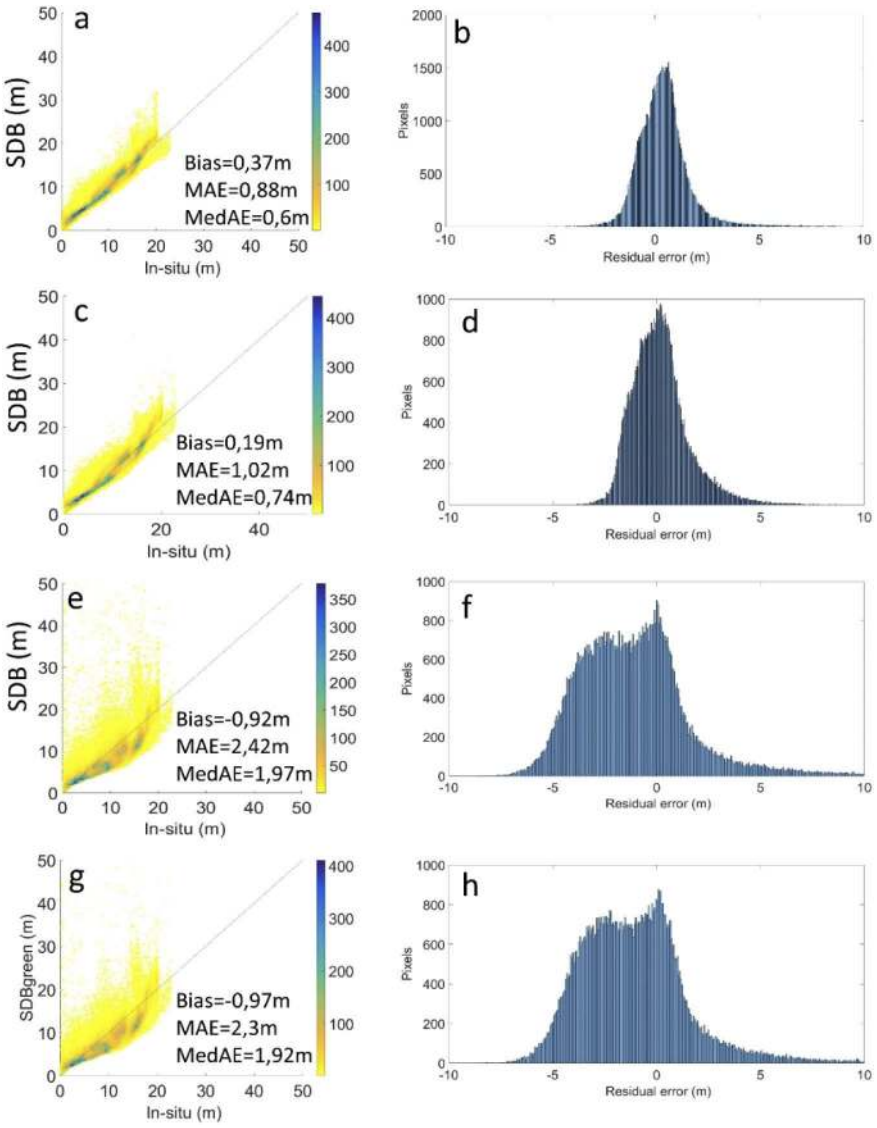

Fig. 4. Scatter of the final SDB composite after the multi-temporal approach (using 13 scenes, see Appendix) in Buck Island using a) ACOLITE EXP, c) ACOLITE DSF, e) C2RCC, and g) C2RCC (composite using only the 5 scenes with severe sun glint, see Appendix); histogram of residuals using b) ACOLITE EXP, d) ACOLITE DSF, f) C2RCC, and h) C2RCC (composite using only the 5 scenes with severe sun glint).

Optics EXPRESS

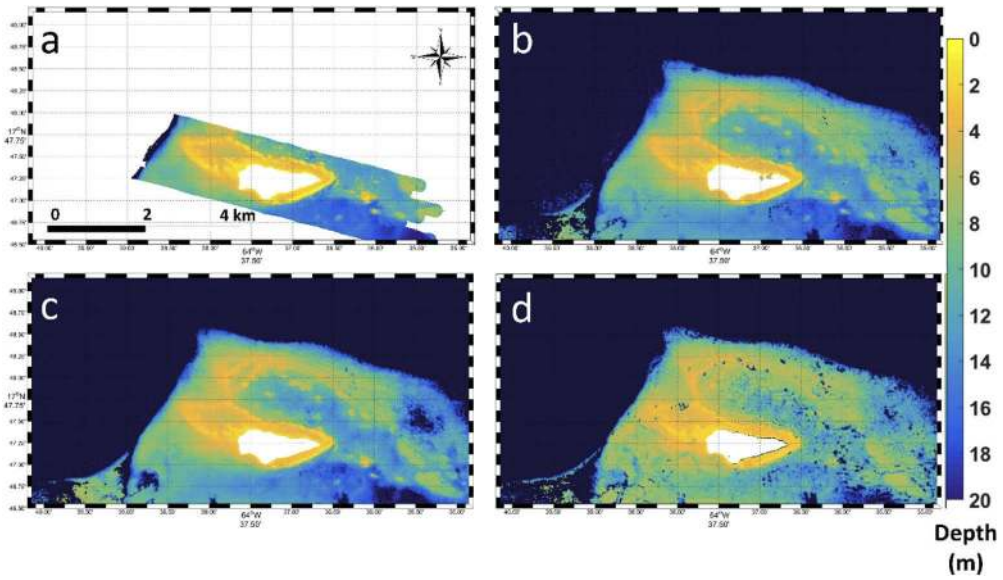

Fig. 5. a) Lidar survey in Buck Island at 1 m spatial resolution, and maps of the final SDB after compositing using b) ACOLITE EXP, c) ACOLITE DSF, and d) C2RCC. The noisier results from C2RCC are visible in the map. Dark blue colour corresponds to optically deep waters.

EXP and DSF, whereas lower values 0.3-0.87 were associated to C2RCC (Table 4). Variability (Coefficient of Variation, CV) between calibration slopes for individual scenes was somewhat higher for C2RCC than for the others. For scene 3 acquired on 17 July 2018, which is located in the eastern side of the swath, sunglint severely affected this study region, and none of the processors, including C2RCC, performed accurately. Culebra, like Buck Island, has a microtidal in this region, so that was not a factor in intercept variation.

Table 3. Summary table with mean and standard deviation (SD) statistics of biases and MedAE for the three AC methods using scene-by-scene calibration or unique single calibration in Culebra Island.

	ACOLITE	EXP	ACOLITE	DSF	C2RCC	
Culebra Island	Scene-by-scene calibration	Single calibration	Scene-by-scene calibration	Single calibration	Scene-by-scene calibration	Single calibration
Mean of scene biases (m)	0.37	-0.2	0.6	0.5	0.1	-0.25
SD of scene biases (m)	0.02	1.71	0.55	1.22	0.72	1.28
Mean of scene MedAE (m)	1.3	1.9	1.3	1.7	2.3	2.1
SD of scene MedAE (m)	0.3	1.16	0.57	0.86	0.9	1.1

The EXP and DSF provided the best overall accuracy achieving median errors of 1.3 m followed by the C2RCC with higher (>75%) median errors of 2.3 m over depths ranging from 0-20 m. The exploratory analysis also allowed us to assess the impact of the AC on the relationship of SDB to ALB data. While each AC technique was capable of generating good results, there are clear inconsistencies in the stability of the results between techniques. The ACOLITE

Optics EXPRESS

processor generated consistent results for all depth ranges, whereas lower performance was found for C2RCC, as can be noted in the accuracy assessment results for each of the individual scenes relative to the in-situ bathymetric validation data (see Tables 8–10 in Appendix, left side). We reported an example using a single optimal scene acquired on 30 January 2019; for data relationships, the associated scatterplots and histogram of residuals are given in Fig. 6. While both ACOLITE models performed similarly with MedAE ~1 m, C2RCC retrieves bathymetry with higher median error of 1.7 m (>70%). ACOLITE processor provided worthwhile improvement at Culebra as was the case of Buck Island. When using a single calibration (30 January 2019), ACOLITE has median errors 35% higher compared to the multi-temporal approach (similar to Buck Island), while for C2RCC differences between the single calibration and multi-temporal approach are smaller (Tables 8–10 in Appendix, right side).

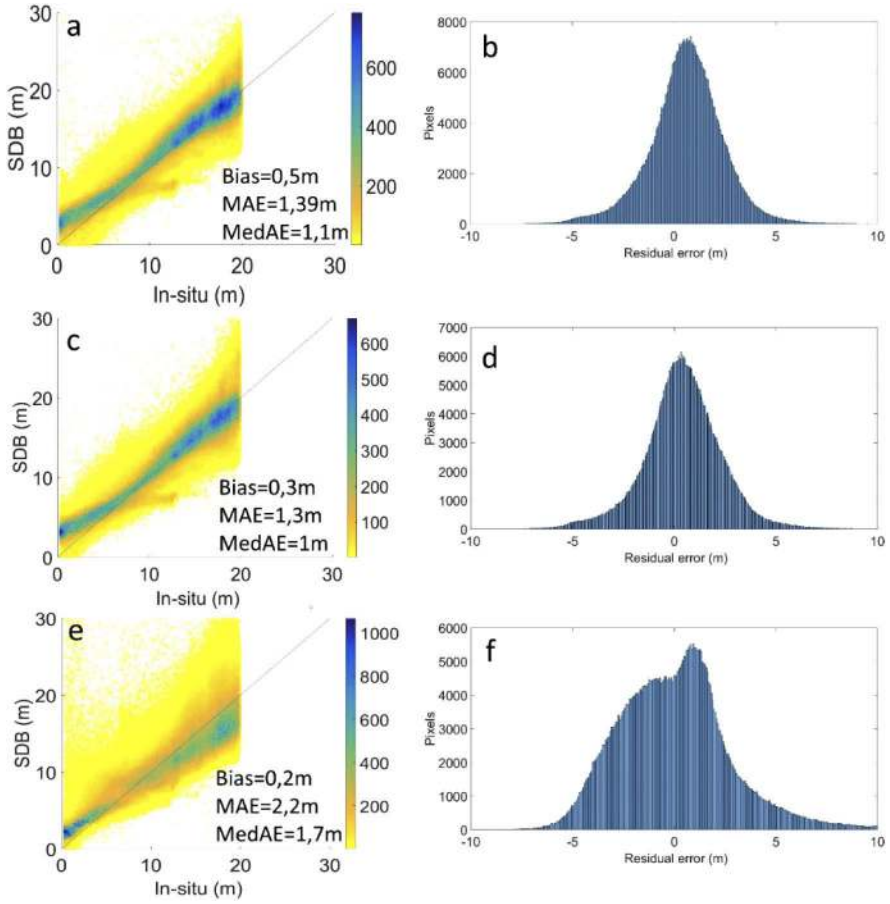

Fig. 6. Examples of scatters for the validation of individual SDB in Culebra Island using a Sentinel-2B image acquired on 30 January 2019 after the AC for a) ACOLITE EXP, c) ACOLITE DSF, and e) C2RCC; and histogram of residuals for b) ACOLITE EXP, d) ACOLITE DSF, and f) C2RCC.

The accuracy for the compositing model and the three AC methods are summarized via the scatterplots and residual diagnostics in Fig. 7, together with SDB maps [Figs. 8(b)–8(d)] compared to lidar data [Fig. 8(a)]. On viewing the diagnostics, some clear trends emerge, where the most accurate model was first EXP (MedAE=0.98 m), then DSF (MedAE=1.3 m), and finally C2RCC (MedAE=2.2 m). It can be observed that the C2RCC model was noisy with

Optics EXPRESS

strong scatter compared to ACOLITE models. The information from residuals also pointed out a normal distribution for both ACOLITE models, whereas C2RCC had a skewed and long-tailed distribution [Fig. 6(f)]. The ACOLITE-derived multi-temporal products also had better final vertical calibration after compositing with r^2=0.97 (26.5x-22) and 0.93 (22.7x-18), for EXP and DSF, respectively, compared to C2RCC with r^2=0.78 (16.5x-13).

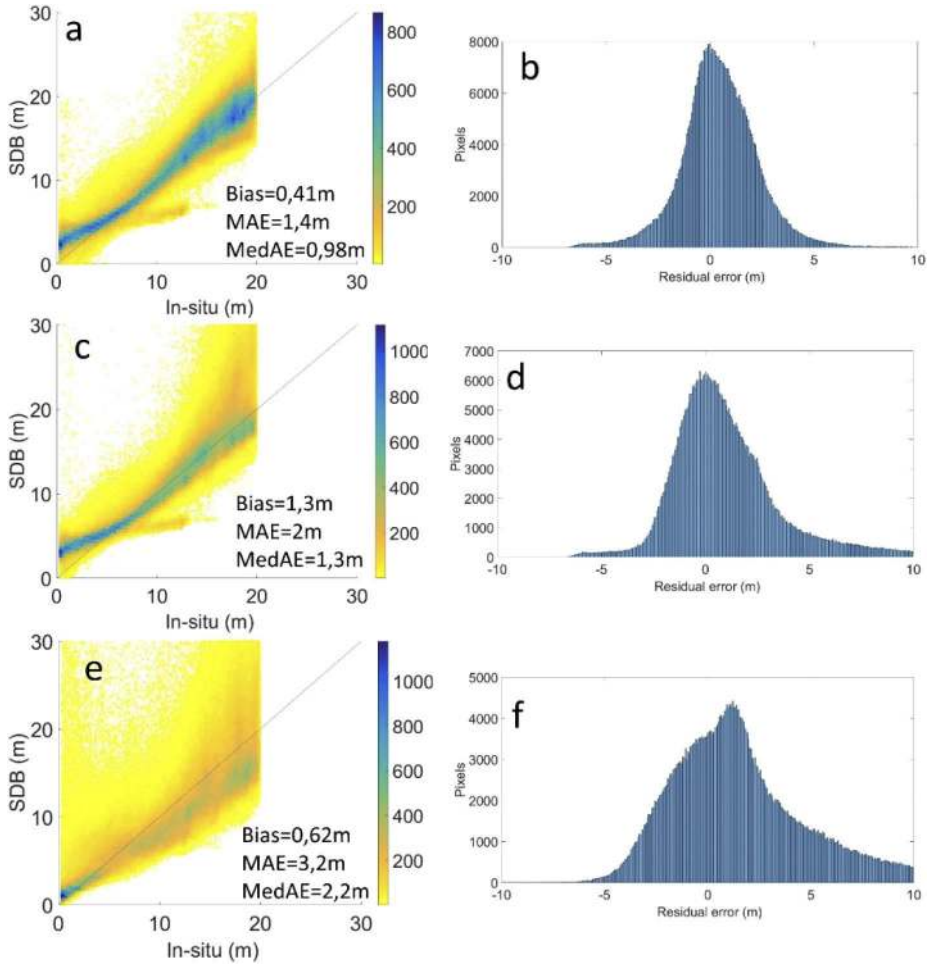

Fig. 7. Scatter of the final SDB composite after the multi-temporal approach in Culebra Island using a) ACOLITE EXP, c) ACOLITE DSF, and e) C2RCC; histogram of residuals using b) ACOLITE EXP, d) ACOLITE DSF, and f) C2RCC.

The ACOLITE models have the highest density point distribution close to the 1:1 line (Fig. 7, left side) or more tightly clustered around a zero residual error [Figs. 7(b), 7(d), vs 7(f) for C2RCC]. These results indicate that ACOLITE always out-performed C2RCC, in terms of average bias and accuracy (overall MedAE and MAE), for single and multi-temporal approaches. The comparison also aimed to validate the spatial patterns of the Sentinel-2 composited SDB, being spatially consistent with the irregular benthic geomorphology derived from the ALB measurements. Overall, SDB maps retrieved the depth gradient with high accuracy as in the ALB from coastal (shallow) to open ocean (deep). The saturated depths (optically deep ocean) were indicated with depths exceeding 20 m, beyond the slope into the open ocean [dark blue in Figs. 8(b)–8(d)].

Optics EXPRESS

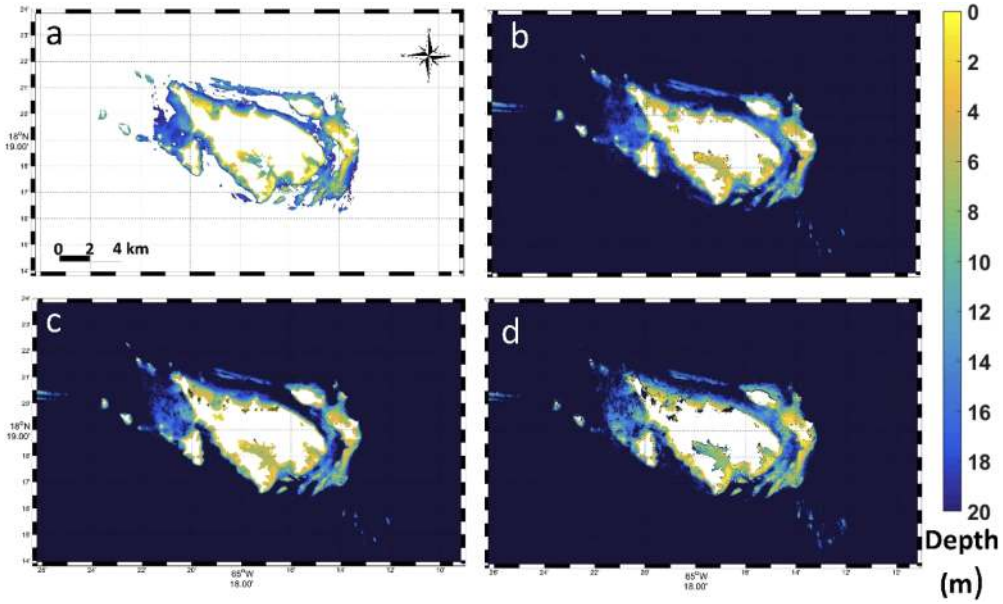

Fig. 8. a) Lidar survey in Culebra Island at 1 m spatial resolution, and maps of the final SDB after compositing using b) ACOLITE EXP, c) ACOLITE DSF, and d) C2RCC. Dark blue colour corresponds to optically deep waters.

4. Discussion

Accurate AC during image pre-processing is extremely important for reliable bathymetric estimation with Sentinel-2 [23,25]. Based on these results, it is important to note that each of the AC processors has strengths and weaknesses related to the AC and sunglint correction. The ACOLITE processor, both EXP and DSF, performed consistently and accurately in both study regions, Buck and Culebra Islands, with lower mean errors for single image approaches, whereas C2RCC corrected with poorer precision, higher noise and errors (>50%). On the other hand, C2RCC was able to retrieve depths from moderately severe sunglint scenes in Buck Island (Fig. 3) whereas ACOLITE EXP and DSF masked out the data (there are limits, C2RCC still could not retrieve in the most heavily glinted scene, July 17, at Culebra). C2RCC might then be useful for a case when essentially only glinted scenes are available during summer, however, with substantial caution about noise [Fig. 3 for single scenes and Figs. 4(g) and 4(h) for composited C2RCC glint only scenes]. If otherwise usable scenes are available, ACOLITE should be used. Even though ACOLITE did not retrieve information during extreme sunglint, higher consistency and less noise was obtained from ACOLITE compared to C2RCC in terms of validation against lidar for the one-year study period (Figs. 2, 3, 6; Tables 5–10). C2RCC is noisier than ACOLITE in both regions and this issue can be observed not only in the several scatter but also in the SDB maps (Fig. 5), where C2RCC showed some bias in different parts of the maps. The noise in C2RCC is also present even in the multi-temporal composites (Figs. 4 and 7). Information of noisier AC processors is a relevant topic for other researchers interested in high-resolution bathymetric maps for a proper detection of detailed small features.

Recent works have demonstrated that ACOLITE produced acceptably accurate estimates of SDB in optically complex waters such as Ireland [25], France [40], Florida [17,24], and North Carolina [29]. Glint-correction algorithms have improved the retrieval accuracy from the sub-optimal image data [26]. Casal et al. [25] evaluated several AC models in Dublin and Mulroy bays for SDB, and indicated that C2RCC was more consistent in handling sunglint in Mulroy Bay

Optics EXPRESS

compared to Sen2Cor, iCOR, and ACOLITE (EXP model only) with scenes around the summer solstice (May to July). Our results in this study are consistent with their outcomes, since we find that C2RCC retrieves more data than ACOLITE during moderately intense sunglint periods. Casal et al. [25] however noted that ACOLITE performed better in Dublin Bay (ACOLITE, r^2=0.68; C2RCC, r^2=0.64), consistent with ACOLITE's design for turbid waters, and the more optically complex waters of Dublin Bay compared to Mulroy Bay. Our recent research has also confirmed ACOLITE as an accurate and consistent model for atmospheric correction of Sentinel-2 imagery in many different turbid environments along the east coast of USA [17,24,29].

Some studies on SDB have used Sentinel-2 data from Level 2 from the SciHub, corrected with Sen2Cor in SNAP [18,28] whereas other researchers applied the Dark Object Subtraction (DOS) to correct for atmospheric signal [46,47,52]. DOS requires assumption of uniform atmosphere and surface reflection, not an optimal condition in these regions. A recent work compared some AC methods (ACOLITE DSF, SeaDAS) when applied to a radiative transfer-based SDB method for one Landsat-8 scene [53]. This research examined only the temporal consistency of the ACs to SDB, and did not address their overall radiometric accuracy. Errors in correcting for Rayleigh scattering could produce bias between individual images, by introducing errors in the blue band (490 nm), which is more sensitive to Rayleigh scattering [26]. Such a bias in one or both of the ACs could cause the difference in calibration slopes between ACOLITE and C2RCC. While further analyses are required, this research indicates that Sentinel-2 data corrected with ACOLITE is a good solution for SDB when scenes without sunglint or minimal sunglint are available. For application to other algorithms that require accurate water reflectance (Rrs), a more exhaustive evaluation of the AC methods against in-situ radiance measurements will be necessary [54–57].

SDB assessment indicated consistence and repeatability between dates in both study areas as the images were acquired within one year. In addition, the results applying the multi-temporal approach for the one-year period demonstrated that the proposed method yield substantial performance improvement compared to individual scenes in Buck (Figs. 4–5) and Culebra (Figs. 7–8) regions. The ACOLITE EXP processor and SDB composited model successfully derived bathymetric information in both regions with MedAE <1 m for depths up to 23 m (limit of lidar surveys). When compared to the classical single image approach, we found the multi-compositing reduced the bathymetry estimation error using both ACOLITE models in these clear water environments. The histograms of errors produced minimum bias and its prediction residual exhibited a random pattern with normal distribution. A recent work with Pleiades in two tropical islands of the northeast Caribbean obtained root mean square errors of 1.39-1.76 m, but their single-scene application was constrained by the presence of clouds and suitable satellite imagery with optimum water surface and water column conditions [58]. Researchers found out after a temporal inspection that summer months provide the best results for SDB [28]. In our case, the best results for both regions depended on the AC model used, but generally, better performances were observed during winter and spring than during summer, which might be caused to some extent by sunglint impact.

The consistency of the ACs means that only the final composited scene required calibration; no calibration is necessary prior to compositing. Also, few training data samples were needed, 25 lidar points in this case for the multi-scene composites; and previous work has shown that this method works with <10 reference points [13,17,24]. To further examine consistency across study areas in the composite calibration, we exchanged the vertical calibration of Buck Island with that for Culebra Island. Figure 9 shows the scatterplots and histogram of residuals, indicating that with the switched calibrations, ACOLITE EXP [Figs. 9(a), 9(g) and DSF in Figs. 9(c), 9(i)] estimated SDB with median errors <1.4 m whereas C2RCC MedAE was 80% higher ~2.5 m [Figs. 9(e), 9(k)]. This information indicates that a common vertical calibration may be possible for this region. Potentially, such a calibration could be applicable to other areas in the region

Optics EXPRESS

that lack field data, but urgently require bathymetry, such as after a hurricane. A recent study showed a similar result when switching composite-based calibrations between Florida and North Carolina coastal waters [29].

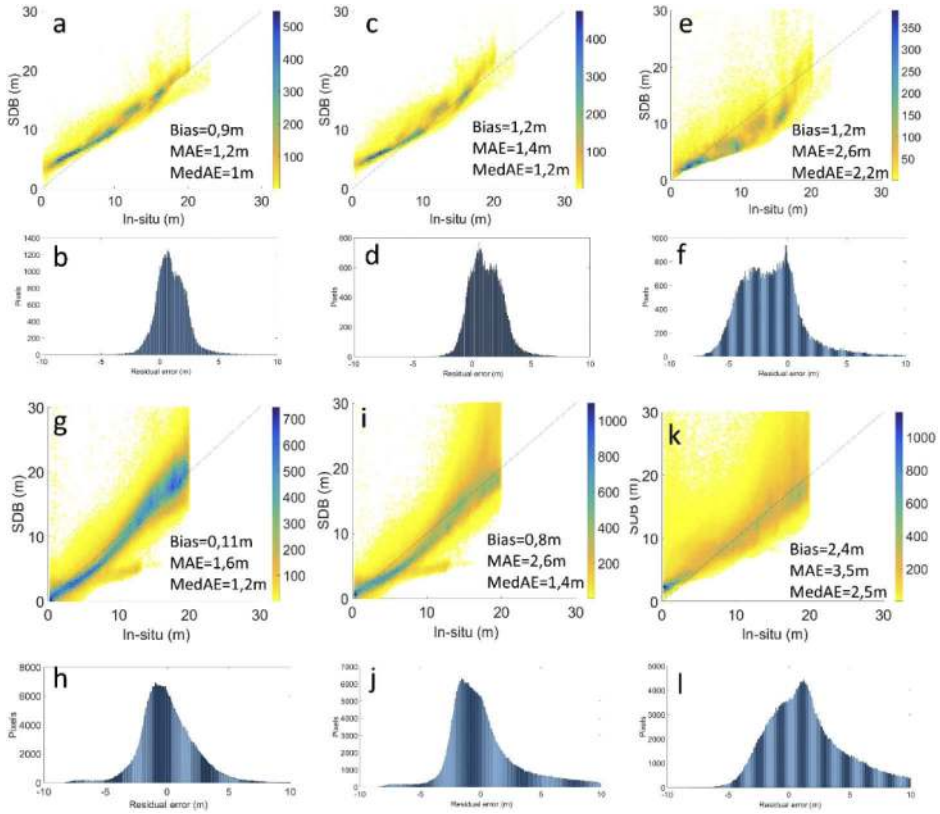

Fig. 9. Scatter of the final SDB composite after the multi-temporal approach in Buck Island applying the vertical calibration from Culebra Island using a) ACOLITE EXP, c) ACOLITE DSF, and e) C2RCC; histogram of residuals using b) ACOLITE EXP, d) ACOLITE DSF, and f) C2RCC; the same for Culebra Island applying the vertical calibration from Buck Island using g) ACOLITE EXP, i) ACOLITE DSF, and k) C2RCC; histogram of residuals using h) ACOLITE EXP, j) ACOLITE DSF, and l) C2RCC.

Unlike the traditional models that manually select the best scene for bathymetry retrieval, our approach used a set of images during a study period, with assumption of minimal change of bottom depth, and implemented an automated model generating a final SDB composite. In this study, the composite product was formed using a time series of Sentinel-2A/B scenes with minimal manual screening (except excluding scenes with extensive cloud cover). A recent paper evaluated global coastal coverage of Sentinel-2 for bathymetric mapping, and found that cloud cover probability is a critical factor, particularly for equatorial regions [59]. Hence, compositing framework represents a major step forward in both the retrieval of spatially usable SDB as well as the automation of bathymetry estimation from optical satellite images. In addition, while this study examined areas of uniform clear water, the proposed compositing methodology was designed to be applied to shallow water with varying water clarity levels and higher turbidity. This approach was demonstrated to mitigate turbidity issues in North Carolina and Florida [29], and we suggest here that it could outperform the standard single scene manual selection strategy, thereby leading to automation of optimal SDB determination.

Optics EXPRESS

Tidal conditions could have minimally affected the accuracy of SDB results in the multi-temporal approach since both areas are located in a microtidal system. The time-domain strategy might suppressed tidal effects to a certain extent; however, the improvement of the methodology by compensating for tidal influence in mesotidal ranges is concern for further investigation. One solution for the multi-temporal approach must be to evaluate only Sentinel-2 scenes that have relatively similar tides (preferable low tides) for all the data sets. For further avenues of research with Sentinel-2, we intend to upscale the study results to more environments (e.g. Mediterranean) with different water and atmospheric conditions in order to evaluate repeatability as well as implement the multi-temporal approach in cloud-based computing platforms such as Google Earth Engine [16,19] or the ESA Coastal Thematic Exploitation Platform Coastal-TEP (https://www.coastal-tep.eu/geobrowser/). The promising transferability of this temporal technique will allow advancement of SDB applications and optimize coastal mapping of bathymetric gaps worldwide, especially in data-poor regions [7]. Additionally, by using the open and free archive of the Sentinel-2 constellation, the framework may allow routine assessment of annual variability in bathymetry, improving assessments of the responses of coastal systems to various hazards, including changes due to climate change. To support navigation, annual SDB maps could be generated and used to track changes in bathymetry in highly dynamic regions. These results will simplify the use of SDB, which may provide a global benefit for a variety of concerns, including ecosystems, fisheries, navigation, and coastal protection.

5. Conclusions

We examined the impact of different AC methods on consistency and error assessment in retrieved SDB using multi-temporal Sentinel-2A/B data over two islands in the Caribbean. Using these AC strategies with the log-ratio SDB algorithm, the bathymetry can be effectively obtained at 10 m spatial resolution with relatively high accuracy through integrating few calibration points (25) from lidar. A combination of AC (ACOLITE EXP, ACOLITE DSF, and C2RCC) and SDB applied to several scenes can considerably enhance coastal SDB estimates, but overall performance depends on the AC processor used. The findings indicated image and AC dependent relationships; the three AC processors provided meaningful and robust results, but ACOLITE always out-performed C2RCC, except in scenes with severe sunglint where ACOLITE masked out the data. SDB products using EXP and DSF indicated consistency and repeatability with accurate results compared to in-situ lidar measurements in a scene-by-scene analysis as well as using only a single calibration equation, demonstrating AC stability. Furthermore, we exhibited the AC is also suitable for a multi-temporal compositing approach, resulting in overall median errors of <1m for depths up to 23 m (limit of lidar surveys). The simple and effective compositing model can be used to successfully generate SDB maps with high reliability and no missing data, outperforming the traditional single image approaches, and without needed calibration of the individual input scenes. This wealth of high-resolution data and standardized pre-processing of atmospheric correction will provide improved quantitative information suitable for coastal monitoring and management at local or regional and from annual to decadal scales.

Appendix

In this Appendix, a list of the Sentinel-2A/B imagery used in this study is presented for each study region in the Caribbean waters (Table 4) as well as the results from the comparison of the Atmospheric Correction procedures ACOLITE EXP (without sunglint correction), ACOLITE DSF (sunglint option), and C2RCC (sunglint option) in Buck (Tables 5–7) and Culebra (Tables 8–10) Islands for each individual scene.

Optics EXPRESS

Table 4. List of Sentinel-2A/B images selected for Buck Island (1-18) and Culebra Island (1-11) during 2018-2019 and coefficient of calibration for the vertical referencing (x is the pseudoSDB or relative SDB before the vertical calibration, so the blue-to-green ratio). The coefficient of determination (r^2) is provided for each calibration as quality control. Some scenes in Buck Island using ACOLITE EXP or DSF were masked out due to intense sunglint (7-10 for both models, 13 also for EXP). Scene 3 in Culebra Island is located in the eastern side of the swath, and sunglint was severely affecting the study region, thus none of the processors performed accurately.

N°	Date	Sensor	ACOLITE EXP	r^2	ACOLITE DSF	r^2	C2RCC	r^2
1	15 Jan. 2018	B	31.6x-28.4	0.97	30.8x-27	0.95	27.4x-23.3	0.92
2	30 Jan. 2018	A	32.5x-29.5	0.98	28.6x-25.6	0.97	34.8x-31.5	0.96
3	9 Feb. 2018	A	35.8x-32.9	0.98	34.8x-32	0.98	31.1x-27	0.89
4	6 Mar. 2018	B	28.8x-24.8	0.95	25.4x-21.6	0.92	26.3x-19.7	0.92
5	11 Mar. 2018	A	35.27x-31.7	0.96	32.6x-29.2	0.97	26.4x-20.9	0.94
6	21 Mar. 2018	A	33.x-29.9	0.96	34.2x-30.6	0.96	25.1x-19.4	0.9
7	10 may 2018	A	-	-	-	-	27.5x-21.3	0.94
8	25 May 2018	B	-	-	-	-	36.7x-28.2	0.94
9	14 Jun. 2018	B	-	-	-	-	30.2x-22	0.89
10	13 Aug. 2018	B	-	-	-	-	26.7x-20.6	0.93
11	23 Aug. 2018	B	34.3x-29.5	0.94	71.8x-67.3	0.97	31.6x-24.4	0.92
12	2 Sep. 2018	B	37x-31.5	0.92	42x-37.3	0.94	32.3x-25.4	0.92
13	17 Sep. 2018	A	-	-	57.2x-53.2	0.96	31.9x-26	0.94
14	2 Oct. 2018	B	42.7x-38	0.98	36.4x-32	0.97	34.7x-29.3	0.93
15	17 Oct 2018	A	50.1x-46.1	0.92	35.3x-30.5	0.90	26.1-21.9	0.58
16	27 Oct. 2018	A	36.5x-31.7	0.98	36.9x-32	0.98	34x-28.5	0.93
17	21 Nov. 218	B	39.4x-36.2	0.95	25.5x-20.8	0.92	19.6x-13.6	0.52
18	21 Dec. 2018	B	27.9x-23.3	0.97	25.1x-21	0.95	26.2×21.7	0.89
1	30 Apr. 2018	A	31.2x-25.2	0.97	30.1x - 24.9	0.97	22.6x- 18.1	0.87
2	4 Jun. 2018	B	31.7x-22.8	0.88	15.8x - 7.4	0.84	31.1x - 29.5	0.72
3	17 Jul. 2018	B	-	-	-	-	-	-
4	2 Oct. 2018	B	68.3x-61.4	0.94	57.3x - 50.7	0.95	33.2x- 29.1	0.3
5	21 Nov. 2018	B	31.4x-25.2	0.98	26.4x - 20.2	0.97	16.6x- 11.6	0.82
6	11 Dec. 2018	B	30.8x-25.9	0.93	27.9x - 22.9	0.9	17.3x-13.3	0.77
7	21 Dec. 2018	B	34.6x-29.7	0.97	32.4x - 27.6	0.97	19.5x- 14.3	0.82
8	15 Jan. 2019	A	24.2x-18.7	0.97	27.1x - 22.3	0.98	21.5x-16.7	0.86
9	30 Jan. 2019	B	30.5x-24.5	0.99	27.2x - 21.3	0.97	19.4x-14	0.83
10	6 Mar. 2019	A	35.5x-30	0.97	27.2x - 21.7	0.84	22.6x-18.1	0.87
11	21 Mar. 2019	B	28.5x- 22.0	0.98	26.4x - 20.4	0.98	31.1x - 29.5	0.72

Optics EXPRESS

Table 5. Statistics (bias, Mean Absolute Error-MAE, and Median Absolute Error-MedAE) for the validation of SDB in Buck Island after the application of the ACOLITE EXP AC method (without sunglint correction); left, scene-by-scene individual calibration, and right, unique calibration using the Sentinel-2B scene number 4 acquired on 6 March 2018 as reference. Some scenes in Buck Island using ACOLITE EXP were masked out due to intense sunglint (images 7-10 and 13).

	Scene by scene calibration			Single calibration		
Number	Bias (m)	MedAE (m)	MAE (m)	Bias (m)	MedAE (m)	MAE (m)
1	0.25	0.8	1.17	0.59	0.91	1.12
2	0.3	0.8	1.14	0.59	1.12	1.23
3	0.27	0.62	0.89	-0.01	1	1.17
4	0.12	0.65	0.87	0.12	0.65	0.87
5	-0.06	0.64	0.83	-0.68	1.13	1.29
6	-1.4	1.43	1.61	-1.1	1.33	1.48
7	-	-	-	-	-	-
8	-	-	-	-	-	-
9	-	-	-	-	-	-
10	-	-	-	-	-	-
11	-0.88	1.3	1.64	-2.4	2.4	2.6
12	0.23	1.05	1.4	-2.25	2.27	2.5
13	-	-	-	-	-	-
14	0.79	1.04	1.23	-1.79	1.84	2
15	0.72	0.96	1.04	-1.3	1.4	1.8
16	0.12	0.71	0.88	-1.73	1.98	2
17	0.46	1.03	1.41	-0.62	0.98	1.17
18	0.73	0.96	1.14	0.19	0.82	0.97
Average	0.12	0.91	1.17	-0.79	1.37	1.55

Optics EXPRESS

Table 6. Statistics (bias, Mean Absolute Error-MAE, and Median Absolute Error-MedAE) for the validation of SDB in Buck Island after the application of the ACOLITE DSF AC method (sunglint correction included); left, scene-by-scene individual calibration, and right, unique calibration using the Sentinel-2B scene number 4 acquired on 6 March 2018 as reference. Some scenes in Buck Island using ACOLITE DSF were masked out due to intense sunglint (images 7-10).

Number	Bias (m)	MedAE (m)	MAE (m)	Bias (m)	MedAE (m)	MAE (m)
1	1	1.23	1.4	-0.19	0.91	1.17
2	0.36	0.84	1.01	0.37	1.05	1.18
3	0.52	0.61	1.07	-0.47	1.2	1.47
4	0	0.71	0.96	0	0.71	0.96
5	0.08	0.7	0.92	-0.93	1.35	1.49
6	-0.15	0.9	1.1	-1.5	1.78	1.87
7	-	-	-	-	-	-
8	-	-	-	-	-	-
9	-	-	-	-	-	-
10	-	-	-	-	-	-
11	0.21	0.89	1.26	-3.96	3.9	4.26
12	0.27	0.91	1.25	-2.7	2.7	2.99
13	0.54	0.89	1.16	-3	3.18	3.47
14	0.53	0.99	1.13	-1.83	1.98	2.16
15	1.15	1.23	1.37	-1	1.39	1.61
16	0.46	0.74	0.97	-2.2	2.4	2.53
17	0.36	0.5	1.23	-0.55	1	1.3
18	0.29	0.95	1.12	0.06	0.92	1.11
Average	0.4	0.86	1.13	-1.2	1.74	1.96

Optics EXPRESS

Table 7. Statistics (bias, Mean Absolute Error-MAE, and Median Absolute Error-MedAE) for the validation of SDB in Buck Island after the application of the C2RCC AC method (sunglint correction included); left, scene-by-scene individual calibration, and right, unique calibration using the Sentinel-2B scene number 4 acquired on 6 March 2018 as reference.

Number	Bias (m)	MedAE (m)	MAE (m)	Bias (m)	MedAE (m)	MAE (m)
1	-0.02	1.36	1.9	2.24	1.98	2.58
2	-0.15	1.94	2.4	1.55	1.61	2.1
3	0.46	1.59	2.32	1.99	1.76	2.4
4	2.28	1.6	2.75	2.28	1.6	2.75
5	-0.03	1.17	1.64	1	1.31	1.77
6	-0.23	1.31	1.71	0.84	1.3	1.79
7	0.29	1.05	1.69	0.53	1.1	1.7
8	1.93	1.66	2.32	-0.83	1.36	1.95
9	0.33	1.4	1.73	-1.5	1.5	2.11
10	0.36	1.17	1.9	0.8	1.2	1.93
11	0.37	1.17	1.69	-0.7	1.38	1.87
12	0.5	1.29	1.91	-0.39	1.5	2
13	0.07	1.16	1.65	0.1	1.4	1.74
14	0.03	1.25	1.75	0.17	1.6	1.91
15	-1.77	2	2.35	0.64	1.44	1.82
16	0.01	1.41	1.83	0.15	1.62	1.96
17	-0.41	1.72	2	1.29	1.53	1.98
18	0.75	1.29	1.9	2.83	2.29	2.98
Average	0.26	1.42	1.96	0.72	1.53	2.1

Table 8. Statistics (bias, Mean Absolute Error-MAE, and Median Absolute Error-MedAE) for the validation of SDB in Culebra Island after the application of the ACOLITE EXP AC method (without sunglint correction); left, scene-by-scene individual calibration, and right, unique calibration using the Sentinel-2B scene acquired on 30 January 2019 as reference. No retrieval was obtained on scene 3 due to the extreme sunglint.

	Scene by scene calibration			Single calibration		
Number	Bias (m)	MedAE (m)	MAE (m)	Bias (m)	MedAE (m)	MAE (m)
1	-0.35	1.37	1.65	-0.48	1.3	1.8
2	-0.26	1.53	2.1	-3.2	3.3	3.6
3	-	-	-	-	-	-
4	1.24	2.3	2.5	-3.2	3.6	4
5	1.2	1.49	1.9	0.8	1.4	1.9
6	0.1	1.14	1.54	1	1.5	1.9
7	0.41	1.26	1.74	0.7	1.7	2
8	0.3	1.04	1.3	2.6	2.6	2.8
9	0.52	1.1	1.39	-	-	-
10	0.64	1	1.3	0.2	1.2	1.4
11	-0.06	1.1	1.44	-0.2	1.2	1.5
Average	0.37	1.3	1.6	-0.2	1.9	2.3

Optics EXPRESS

Table 9. Statistics (bias, Mean Absolute Error-MAE, and Median Absolute Error-MedAE) for the validation of SDB in Culebra Island after the application of the ACOLITE DSF AC method (sunglint correction included); left, scene-by-scene individual calibration, and right, unique calibration using the Sentinel-2B scene acquired on 30 January 2019 as reference. No retrieval was obtained on scene 3 due to the extreme sunglint.

Number	Bias (m)	MedAE (m)	MAE (m)	Bias (m)	MedAE (m)	MAE (m)
1	0.03	1.23	1.79	0.1	1.4	1.9
2	0.54	1.67	2.3	1.2	1.6	2.9
3	-	-	-	-	-	-
4	1.5	2.4	3	-2.8	3.2	3.6
5	1.4	1.5	2.3	1.4	1.6	2.3
6	0.3	1.1	1.7	1	1.5	1.9
7	0.3	1.2	1.8	0.7	1.8	2
8	0.2	0.9	1.2	1.3	1.6	1.8
9	0.3	1	1.3	-	-	-
10	1.3	1.3	1.9	1.6	1.6	2.2
11	0.33	1.1	1.6	0.5	1.2	1.7
Average	0.6	1.3	1.7	0.5	1.7	2.2

Table 10. Statistics (bias, Mean Absolute Error-MAE, and Median Absolute Error-MedAE) for the validation of SDB in Culebra Island after the application of the C2RCC AC method (sunglint correction included); left, scene-by-scene individual calibration, and right, unique calibration using the Sentinel-2B scene acquired on 30 January 2019 as reference. No retrieval was obtained on scene 3 due to the extreme sunglint.

Number	Bias (m)	MedAE (m)	MAE (m)	Bias (m)	MedAE (m)	MAE (m)
1	-0.11	2.1	3.1	-0.4	2.1	2.9
2	-1.8	3.5	4	-1.5	2.5	3
3	-	-	-	-	-	-
4	-1.7	2.8	3.9	-3.1	4	4.5
5	-0.4	2.2	2.8	0.8	1.9	2.8
6	-0.9	3	3.2	.4	1.9	2.7
7	0.1	2	2.9	0.4	1.9	2.7
8	-0.3	1.8	2.3	1.8	1.8	2.7
9	0.2	1.7	2.2	-	-	-
10	0.3	1.6	2.3	0.1	1.6	2.3
11	-0.7	1.8	2.3	-0.8	1.8	2.4
Average	0.1	2.3	2.9	-0.25	2.1	2.9

Optics EXPRESS

Funding

National Oceanic and Atmospheric Administration (NRC postdoctoral Research RAP, 2017-2019); Ministerio de Ciencia, Innovación y Universidades (Sen2Coast Project, RTI2018-098784-J-I00).

Acknowledgments

We thank the European Space Agency, the European Commission and the Copernicus programme for distributing Sentinel-2 imagery. Thanks to the National Oceanic and Atmospheric Administration and the National Geodetic Survey for providing the valuable high-resolution lidar data used for this study. The authors acknowledge the three anonymous reviewers, whose comments helped to greatly improve an earlier version of this manuscript.

Disclosures

The authors declare no conflicts of interest.

References

1. Coastal and Marine Ecosystems-Marine Jurisdictions: Coastline Length. (https://web.archive.org/web/20120419075053/http://earthtrends.wri.org/text/coastal-marine/variable-61.html) (accessed on 15 November 2019).
2. CIESIN-Center for International Earth Science Information Network. Gridded Population of the World Version 3 (GPWv3), CIESIN: Palisades, NY, USA, 2005.
3. T. Heege, M. Bergin, K. Hartmann, and K. Schenk, "Satellite Services for Coastal Applications," In *Ocean Solutions, Earth Solutions*, D. J. Wright, Ed. Esri, Redlands, CA, USA, 2016357-368 (2016).
4. R. J. Nicholls, P. P. Wong, V. Burkett, J. Codignotto, and J. Ha, "Coastal systems and low-lying areas," *Clim. Chang. 2007 Impacts, Adapt. Vulnerability. Contribution of Working Group II to the Fourth Assessment Report of the Intergovernmental Panel on Climate Change*, M. L. Parry, O. F. Canziani, J. P. Palutikof, P. J. van der Linden, and C. E. Hanson, eds., Cambridge University, Cambridge, UK, 315–356 (2007).
5. L. Mayer, M. Jakobsson, G. Allen, B. Dorschel, R. Falconer, V. Ferrini, G. Lamarche, H. Snaith, and P. Weatherall, "The Nippon Foundation-GEBCO seabed 2030 project: The quest to see the world's oceans completely mapped by 2030," Geosciences **8**(2), 63 (2018).
6. International Hydrographic Organization, Status of Hydrographic Surveying and Charting Worldwide (IHO/OHI Publication C-55), International Hydrographic Organization (2018).
7. A. C. Wölfl, H. Snaith, S. Amirebrahimi, C. W. Devey, B. Dorschel, V. Ferrini, V. A. I. Huvenne, M. Jakobsson, J. Jencks, G. Johnson, G. Lamarche, L. Mayer, D. Millar, T. H. Pedersen, K. Picard, A. Reitz, T. Schmitt, M. Visbeck, P. Weatherall, and R. Wigley, "Seafloor mapping - The challenge of a truly global ocean bathymetry," Front. Mar. Sci. **6**, 283 (2019).
8. M. W. Beck, I. J. Losada, P. Menéndez, B. G. Reguero, P. Díaz-Simal, and F. Fernández, "The global flood protection savings provided by coral reefs," Nat. Commun. **9**(1), 1–9 (2018).
9. D. C. Mason, C. Gurney, and M. Kennett, "Beach topography mapping - a comparison of techniques," J. Coast. Conserv. **6**(1), 113–124 (2000).
10. J. Gao, "Bathymetric mapping by means of remote sensing: Methods, accuracy and limitations," Prog. Phys. Geogr. **33**(1), 103–116 (2009).
11. D. Lyzenga, "Passive remote sensing techniques for mapping water depth and bottom features," Appl. Opt. **17**(3), 379–383 (1978).
12. Z. Lee, K. L. Carder, C. D. Mobley, R. G. Steward, and J. S. Patch, "Hyperspectral remote sensing for shallow waters: 2 Deriving bottom depths and water properties by optimization," Appl. Opt. **38**(18), 3831–3843 (1999).
13. R. P. Stumpf, K. Holderied, and M. Sinclair, "Determination of water depth with high-resolution satellite imagery over variable bottom types," Limnol. Oceanogr. **48**(1part2), 547–556 (2003).
14. A. G. Dekker, S. R. Phinn, J. Anstee, P. Bissett, V. E. Brando, B. Casey, P. Fearns, J. Hedley, W. Klonowski, Z. P. Lee, M. Lynch, M. Lyons, C. Mobley, and C. Roelfsema, "Intercomparison of shallow water bathymetry, hydro-optics, and benthos mapping techniques in Australian and Caribbean coastal environments," Limnol. Oceanogr. Methods **9**(9), 396–425 (2011).
15. S. M. Hamylton, J. D. Hedley, and R. J. Beaman, "Derivation of high-resolution bathymetry from multispectral satellite imagery: A comparison of empirical and optimisation methods through geographical error analysis," Remote Sens. **7**(12), 16257–16273 (2015).
16. D. Traganos, D. Poursanidis, B. Aggarwal, N. Chrysoulakis, and P. Reinartz, "Estimating satellite-derived bathymetry (SDB) with the Google Earth Engine and sentinel-2," Remote Sens. **10**(6), 859 (2018).
17. I. Caballero, R. P. Stumpf, and A. Meredith, "Preliminary Assessment of Turbidity and Chlorophyll Impact on Bathymetry Derived from Sentinel-2A and Sentinel-3A Satellites in South Florida," Remote Sens. **11**(6), 645 (2019).

Optics EXPRESS

18. D. Poursanidis, D. Traganos, N. Chrysoulakis, and P. Reinartz, "Cubesats allow high spatiotemporal estimates of satellite-derived bathymetry," Remote Sens. **11**(11), 1299 (2019).
19. T. Sagawa, Y. Yamashita, T. Okumura, and T. Yamanokuchi, "Satellite derived bathymetry using machine learning and multi-temporal satellite images," Remote Sens. **11**(10), 1155 (2019).
20. European Space Agency, 2015, Sentinel-2 User Handbook, ESA Standard Document Paris, France (https://sentinel.esa.int/documents/247904/685211/Sentinel-2_User_Handbook) (accessed on 20 December 2019).
21. European Space Agency, 2017, Sentinel-2 MSI Technical Guide (https://earth.esa.int/web/sentinel/technical-guides/sentinel-2-msi) (accessed on 20 December 2019).
22. A. Chybicki, "Mapping South Baltic Near-Shore Bathymetry Using Sentinel-2 Observations," Polish Marit. Res. **24**(3), 15–25 (2017).
23. J. D. Hedley, C. Roelfsema, V. Brando, C. Giardino, T. Kutser, S. Phinn, P. J. Mumby, O. Barrilero, J. Laporte, and B. Koetz, "Coral reef applications of Sentinel-2: Coverage, characteristics, bathymetry and benthic mapping with comparison to Landsat 8," Remote Sens. Environ. **216**, 598–614 (2018).
24. I. Caballero and R. P. Stumpf, "Retrieval of nearshore bathymetry from Sentinel-2A and 2B satellites in South Florida coastal waters," Estuar. Coast. Shelf Sci. **226**, 106277 (2019).
25. G. Casal, X. Monteys, J. Hedley, P. Harris, C. Cahalane, and T. McCarthy, "Assessment of empirical algorithms for bathymetry extraction using Sentinel-2 data," Int. J. Remote Sens. **40**(8), 2855–2879 (2019).
26. E. J. Botha, V. E. Brando, and A. G. Dekker, "Effects of per-pixel variability on uncertainties in bathymetric retrievals from high-resolution satellite images," Remote Sens. **8**(6), 459 (2016).
27. S. Chu, L. Cheng, X. Ruan, Q. Zhuang, X. Zhou, M. Li, and Y. Shi, "Technical Framework for Shallow-Water Bathymetry With High Reliability and No Missing Data Based on Time-Series Sentinel-2 Images," IEEE Trans. Geosci. Remote Sens. **57**(11), 8745–8763 (2019).
28. E. Evagorou, C. Mettas, A. Agapiou, K. Themistocleous, and D. Hadjimitsis, "Bathymetric maps from multi-temporal analysis of Sentinel-2 data: The case study of Limassol, Cyprus," Adv. Geosci. **45**, 397–407 (2019).
29. I. Caballero and R. P. Stumpf, "Towards routine mapping of shallow bathymetry in environments with variable turbidity: contribution of Sentinel-2A/B satellites mission," Remote Sens. **12**(3), 451 (2020).
30. J. A. Goodman, Z. P. Lee, and S. L. Ustin, "Influence of atmospheric and sea-surface corrections on retrieval of bottom depth and reflectance using a semi-analytical model: A case study in Kaneohe Bay, Hawaii," Appl. Opt. **47**(28), F1–F11 (2008).
31. J. F. Bramante, D. K. Raju, and T. M. Sin, "Multispectral derivation of bathymetry in Singapore's shallow, turbid waters," Int. J. Remote Sens. **34**(6), 2070–2088 (2013).
32. International Ocean-Colour Coordinating Group. Atmospheric Correction for Remotely-Sensed Ocean-Colour Products. Reports of the International Ocean-Colour Coordinating Group, No. 10, IOCCG, edited by M. Wang, 78. Dartmouth, Canada (2010).
33. Q. Vanhellemont and K. Ruddick, "Turbid wakes associated with offshore wind turbines observed with Landsat 8," Remote Sens. Environ. **145**, 105–115 (2014).
34. Q. Vanhellemont and K. Ruddick, "Advantages of high quality SWIR bands for ocean colour processing: Examples from Landsat-8," Remote Sens. Environ. **161**, 89–106 (2015).
35. Q. Vanhellemont and K. Ruddick, "Acolite for Sentinel-2: Aquatic applications of MSI imagery," Eur. Sp. Agency, (Special Publ.), ESA SP SP-740, 9–13 (2016).
36. Q. Vanhellemont and K. Ruddick, "Atmospheric correction of metre-scale optical satellite data for inland and coastal water applications," Remote Sens. Environ. **216**, 586–597 (2018).
37. Q. Vanhellemont, "Adaptation of the dark spectrum fitting atmospheric correction for aquatic applications of the Landsat and Sentinel-2 archives," Remote Sens. Environ. **225**, 175–192 (2019).
38. R. Doerffer and H. Schiller, "The MERIS case 2 water algorithm," Int. J. Remote Sens. **28**(3-4), 517–535 (2007).
39. C. Brockmann, R. Doerffer, M. Peters, S. Kerstin, S. Embacher, and A. Ruescas, "Evolution of the C2RCC neural network for Sentinel 2 and 3 for the retrieval of ocean colour products in normal and extreme optically complex waters," In Living Planet Symposium ESA **740**, 54 (2016).
40. E. Salameh, F. Frappart, R. Almar, P. Baptista, G. Heygster, B. Lubac, D. Raucoules, L. P. Almeida, E. W. J. Bergsma, S. Capo, M. De Michele, D. Idier, Z. Li, V. Marieu, A. Poupardin, P. A. Silva, I. Turki, and B. Laignel, "Monitoring Beach Topography and Nearshore Bathymetry Using Spaceborne Remote Sensing: A Review," Remote Sens. **11**(19), 2212 (2019).
41. E. A. Hernandez-Delgado, L. Alicea-Rodriguez, C. G. Toledo, and A. M. Sabat, "Baseline characterization of coral reefs and fish communities within the proposed Culebra Island marine fishery reserve, Puerto Rico," In Proceedings of the Gulf and Caribbean Fisheries Institute **51**, 537–555 (2000).
42. M. S. Kendal, M. E. Monaco, K. R. Buja, J. D. Christensen, C. R. Kruer, M. Finkbeiner, and R. A. Warner, "Methods Used to Map the Benthic Habitats of Puerto Rico," NOAA National Ocean Service Center for Coastal Monitoring and Assessment Biogeography Team, Report 45 (2001).
43. N. Pahlevan, S. Sarkar, B. A. Franz, S. V. Balasubramanian, and J. He, "Sentinel-2 MultiSpectral Instrument (MSI) data processing for aquatic science applications: Demonstrations and validations," Remote Sens. Environ. **201**, 47–56 (2017).
44. A. Minghelli-Roman, A. Goreac, S. Mathieu, M. Spigai, and P. Gouton, "Comparison of bathymetric estimation using different satellite images in coastal sea waters," Int. J. Remote Sens. **30**(21), 5737–5750 (2009).

Optics EXPRESS

45. H. Mohamed, M. Salah, K. Nadaoka, and M. Zahran, "Assessment of proposed approaches for bathymetry calculations using multispectral satellite images in shallow coastal/lake areas: a comparison of five models," Arab. J. Geosci. **10**(2), 42 (2017).
46. J. M. Kerr and S. Purkis, "An algorithm for optically-deriving water depth from multispectral imagery in coral reef landscapes in the absence of ground-truth data," Remote Sens. Environ. **210**, 307–324 (2018).
47. C. Cahalane, A. Magee, X. Monteys, G. Casal, J. Hanafin, and P. Harris, "A comparison of Landsat 8, RapidEye and Pleiades products for improving empirical predictions of satellite-derived bathymetry," Remote Sens. Environ. **233**, 111414 (2019).
48. R. Chénier, R. Ahola, M. Sagram, M. A. Faucher, and Y. Shelat, "Consideration of level of confidence within multi-approach satellite-derived bathymetry," ISPRS Int. J. Geo-Information **8**(1), 48 (2019).
49. E. C. Geyman and A. C. Maloof, "A Simple Method for Extracting Water Depth From Multispectral Satellite Imagery in Regions of Variable Bottom Type," Earth Sp. Sci. **6**(3), 527–537 (2019).
50. T. D. Leder, N. Leder, and J. Peros, "Satellite derived bathymetry survey method – Example of Hramina bay," Trans. Marit. Sci. **8**(1), 99–108 (2019).
51. J. Li, D. E. Knapp, S. R. Schill, C. Roelfsema, S. Phinn, M. Silman, J. Mascaro, and G. P. Asner, "Adaptive bathymetry estimation for shallow coastal waters using Planet Dove satellites," Remote Sens. Environ. **232**, 111302 (2019).
52. A. P. Yunus, J. Dou, X. Song, and R. Avtar, "High Resolution Sentinel-2 Images for Improved Bathymetric Mapping of Coastal and Lake Environments," Preprints 2019020270 (2019).
53. I. C. Olayinka and A. Knudby, "Satellite-derived bathymetry using a radiative transfer-based method: A comparison of different atmospheric correction methods," In OCEANS 2019 MTS/IEEE SEATTLE IEEE, 1–4 (2019).
54. G. Doxani, E. Vermote, J. C. Roger, F. Gascon, S. Adriaensen, D. Frantz, O. Hagolle, A. Hollstein, G. Kirches, F. Li, J. Louis, A. Mangin, N. Pahlevan, B. Pflug, and Q. Vanhellemont, "Atmospheric correction inter-comparison exercise," Remote Sens. **10**(3), 352 (2018).
55. A. Ansper and K. Alikas, "Retrieval of chlorophyll a from Sentinel-2 MSI data for the European Union water framework directive reporting purposes," Remote Sens. **11**(1), 64 (2018).
56. M. Pereira-Sandoval, A. Ruescas, P. Urrego, A. Ruiz-Verdú, J. Delegido, C. Tenjo, X. Soria-Perpinyà, E. Vicente, J. Soria, and J. Moreno, "Evaluation of atmospheric correction algorithms over Spanish inland waters for sentinel-2 multi spectral imagery data," Remote Sens. **11**(12), 1469 (2019).
57. M. A. Warren, S. G. H. Simis, V. Martinez-Vicente, K. Poser, M. Bresciani, K. Alikas, E. Spyrakos, C. Giardino, and A. Ansper, "Assessment of atmospheric correction algorithms for the Sentinel-2A MultiSpectral Imager over coastal and inland waters," Remote Sens. Environ. **225**, 267–289 (2019).
58. S. Pike, D. Traganos, D. Poursanidis, J. Williams, K. Medcalf, P. Reinartz, and N. Chrysoulakis, "Leveraging Commercial High-Resolution Multispectral Satellite and Multibeam Sonar Data to Estimate Bathymetry: The Case Study of the Caribbean Sea," Remote Sens. **11**(15), 1830 (2019).
59. E. W. J. Bergsma and R. Almar, "Coastal coverage of ESA' Sentinel 2 mission," Adv. Space Res. In Press (2020).